Rare Metal Materials and Engineering
Volume 52, Issue 1, January 2023
Available online at www.rmme.ac.cn

Science Press

Cite this article as: Luo Yulun, Zhang Dingfei, Hua Jianrong, et al. Effect of High Y Addition on Microstructure and Mechanical Properties of Mg-2Zn-1Mn Alloy[J]. Rare Metal Materials and Engineering, 2023, 52(01): 54-62.

ARTICLE

Effect of High Y Addition on Microstructure and Mechanical Properties of Mg-2Zn-1Mn Alloy

Luo Yulun[1,2], Zhang Dingfei[1,2], Hua Jianrong[1,2], Dai Qimin[1,2], Zhong Shiyu[1,2], Xu Junyao[1,2], Hu Guangshan[3], Jiang Bin[1,2], Pan Fusheng[1,2]

[1] College of Materials Science and Engineering, Chongqing University, Chongqing 400045, China; [2] National Engineering Research Center for Magnesium Alloys, Chongqing University, Chongqing University, Chongqing 400044, China; [3] College of Information Science and Engineering, Jiaxing University, Jiaxing 314001 China

Abstract: The microstructure and mechanical properties of Mg-2Zn-1Mn-*x*Y (*x*=0, 1, 3, 5, 7, wt%) alloy were studied by optical microscope (OM), X-ray diffractometer (XRD), X-ray fluorescence spectrometer (XRF), electron probe microanalyzer (EPMA), scanning electron microscope (SEM), electron backscatter diffractometer (EBSD), transmission electron microscope (TEM), and uniaxial tensile tests. Results show that the secondary phases of as-cast alloys are changed from Mg_7Zn_3 to $Mg_3Zn_3Y_2$ and finally transformed to $Mg_{12}ZnY$ with the addition of Y element. Although Y addition hinders the dynamic recrystallization process and therefore refines the grains, the excess Y addition cannot further refine the grains. Meanwhile, the ductility of as-extruded Mg-2Zn-1Mn alloy is increased and then decreased with the addition of Y element, which may be attributed to the synergistic effect of texture orientation and grain coarsening. Besides, the strength enhancement is mainly attributed to grain refinement strengthening and secondary phase strengthening. The Mg-2Zn-1Mn-7Y alloy has the optimal mechanical properties: the ultimate tensile strength is 357 MPa, yield strength is 262 MPa, and elongation is 14%.

Key words: Mg-Zn-Mn-Y; microstructure; mechanical properties; texture

Magnesium alloys, as the light structural materials, have excellent potential in the aerospace, transportation, and electronic device industries due to their high specific strength, high specific stiffness, and good castability[1–3]. However, the application of Mg alloys is restricted due to their low strength and poor formability. Alloying is generally considered as an effective method to improve the microstructure and mechanical properties of Mg alloys. It is reported that after the addition of Zn and Mn into Mg alloy, the high-strength alloy can be obtained with low cost[4–5]. In addition, Zhang[4] and Liang[6] et al found that the strength of Mg-Zn-Mn alloys is increased with increasing the Zn content. Yield strength (YS) of 213 MPa and ultimate tensile strength (UTS) of 312 MPa can be achieved for Mg-6Zn-Mn alloys. It is also reported that the elongation (EL) of Mg-2Zn-1Mn alloy is nearly 20%, which is much higher than that of other alloys with high Zn content. However, the strength of Mg-2Zn-1Mn alloy is relatively low[7–9].

Rare earth (RE) elements have excellent mechanical properties at ambient temperature, which have been widely used to moderate Mg alloys[10–11]. It is reported that different Zn/Y atomic ratios can lead to the formation of different strengthening phases in Mg-Zn-Y alloys. The secondary phase is transformed from Mg_3Zn_6Y (I-phase) to $Mg_3Zn_3Y_2$ (W-phase) and finally to $Mg_{12}ZnY$ (LPSO-phase) with decreasing the Zn/Y atomic ratio from 4.38 to 1.10[12–14]. LPSO-phase acts as the unique strengthening phase in Mg alloys, which significantly promotes the grain refinement and improves the strength and fracture resistance of Mg alloys through the tight connection between LPSO-phase and Mg matrix[15–16]. Yoshimoto et al[17] reported that the as-extruded $Mg_{96}Zn_2Y_2$ (at%) alloy has high YS of 390 MPa due to the presence of the

Received date: March 05, 2022
Foundation item: National Key Research and Development Program of China (2019YFC1520303); Natural Science Foundation of Zhejiang Province (LQ18E010003); Chongqing Science and Technology Commission (cstc2019jscx-mbdxX0031)
Corresponding author: Zhang Dingfei, Ph. D., Professor, College of Materials Science and Engineering, Chongqing University, Chongqing 400045, P. R. China, Tel: 0086-23-65112491, E-mail: zhangdingfei@cqu.edu.cn

14H-LPSO phase. Hao et al[18] also found that the as-extruded $Mg_{94}Zn_{2.5}Y_{2.5}Mn_1$ (at%) alloy with 14H-LPSO phase exhibits higher strength but lower ductility, compared with that without 14H-LPSO phase. Xu et al[19] found that when the W-phase content exceeds 17.5vol%, W-phase forms obviously coarsened net-like microstructure at the grain boundaries and degrades the mechanical properties of alloys. Meanwhile, Wang et al[20] found that net-like W-phase can broken into particles during the hot extrusion, which activates the particle-stimulated nucleation (PSN) to refine grains, thus improving the strength and ductility.

Therefore, it can be concluded that the recrystallized grain refinement and strengthening phases can be obtained by the addition of Zn, Mn, and Y elements into Mg alloys, thereby improving the mechanical properties of Mg alloys. The Mg-Zn-Mn-Y alloys with low ratio of Y to Zn have been widely researched. However, the investigation of Mg alloys with high Y content is rarely reported. It is reported that the mechanical properties of Mg-2Zn-1Mn alloy can be effectively improved through the trace addition of Y element[21]. In this research, the effect of high Y contents on microstructure and mechanical properties of Mg-2Zn-1Mn alloys was investigated.

1 Experiment

The material used in this research was Mg-2Zn-1Mn-*x*Y (wt%) alloy. Firstly 0wt%, 1wt%, 3wt%, 5wt%, and 7wt% Y element was added into the Mg-2Zn-1Mn alloy, and they were named as ZM21, ZMW211, ZMW213, ZMW215, and ZMW217, respectively. The chemical composition of as-cast billets were analyzed by X-ray fluorescence spectrometer (XRF, XRF-1800) on the cross sections with diameter of 32 mm and length of 5 mm. The results are listed in Table 1. In order to eliminate the segregation of components, homogenization treatment was conducted at 500 °C for 12 h and 420 °C for 12 h for the alloy billets with and without Y addition, respectively. Then the specimens were air-cooled. Afterwards, the homogenized alloy billets were extruded at 450 °C with extrusion ratio of 25:1 and extrusion speed of 20 mm/s.

The as-cast and hot-extruded alloy specimens were ground for metallographic observations. The as-extruded specimens were observed along the direction parallel to the extrusion direction. The phase analysis of specimens was performed by X-ray diffractometer (XRD, PANalytical X'Pert Powder) with Cu-Kα radiation, scanning rate of 4°/min, and scanning angle of 10°–90°. The microstructure characterization of specimens was observed by optical microscope (OM, CLSM), scanning electron microscope (SEM, Quattro S), and transmission electron microscope (TEM, Talos F200s). The electron probe microanalyzer (EPMA, JXA-8530F Plus) was used to characterize the element distribution. Then, the energy dispersive spectroscope (EDS) was used to identify the secondary phases observed by TEM and SEM. Electron backscatter diffractometer (EBSD, JEOL JSM-7800F) was used at 20 kV with step size of 0.6 μm. The crystal orientation was analyzed by Channel 5 software. The high-angle annular dark field (HAADF) TEM was also used.

The specimens for the tensile tests were machined into the ones with a gauge dimension of *Φ*5 mm×35 mm and a total length of 70 mm, according to GB/T 228-2002 standard. Three specimens were selected for each test, and average value of the testing results was used for analysis.

Table 1 Chemical composition of as-cast Mg-2Zn-1Mn-*x*Y alloys (wt%)

Alloy	Zn	Mn	Y	Mg
ZM21	2.25	0.85	0.00	Bal.
ZMW211	1.85	1.32	0.90	Bal.
ZMW213	2.18	0.93	2.39	Bal.
ZMW215	1.95	1.54	4.85	Bal.
ZMW217	1.89	1.56	6.70	Bal.

2 Results and Discussion

2.1 Microstructure of as-cast Mg-2Zn-1Mn-*x*Y alloys

Fig. 1 shows OM microstructures of different as-cast Mg-2Zn-1Mn-*x*Y alloys. It can be seen that compared with the case in ZM21 alloy, the Y addition refines the dendrite spacing and effectively improves the continuity between dendrites. However, as shown in Fig. 1d and 1e, the effect of dendrite refinement is decreased with further increasing the Y addition. As shown in Fig. 2a, a few bright phase particles exist in the as-cast ZM21 alloy, which is composed of Mg-Zn binary phase particles and Mn particles, according to EPMA mapping results. In addition, some other phases consisting of Mg, Zn, and Y elements can also be observed after Y addition. The morphology and size of phases are changed with increasing the Y content, as shown in Fig.2b–2e.

Fig. 3 shows XRD patterns of as-cast Mg-2Zn-1Mn-*x*Y alloys. It is found that the as-cast ZM21 alloy is mainly composed of Mg_7Zn_3, α-Mn, and α-Mg phases, and new diffraction peaks can be detected after Y addition. The diffraction peaks of W-phase can be detected after 1wt% Y addition. With further increasing the Y content, the diffraction peak intensity of W-phase is decreased. In contrast, the diffraction peak intensity of LPSO-phase increases, and the LPSO-phase becomes the main secondary phase. According to SEM microstructures of as-cast alloys (Fig. 4), the granular secondary phase in ZM21 alloy firstly changes to net-work structure and then to lamellar structure after Y addition. It is worth noting that both the W-phase and LPSO-phase appear in ZMW213 alloy (Fig. 4c). It is found that some secondary phase particles with big sizes grow around LPSO-phase. Based on EDS analysis and the results in Ref. [22–23], the particles are considered as Y-rich particles, as shown in Fig.4f.

2.2 Microstructure of as-extruded Mg-2Zn-1Mn-*x*Y alloys

Fig. 5 shows SEM microstructures of as-extruded Mg-2Zn-1Mn-*x*Y alloys, and the observed surface is parallel to the extrusion direction (ED). After homogenous treatment for ZMW211 alloy, the remaining W-phase is crushed during

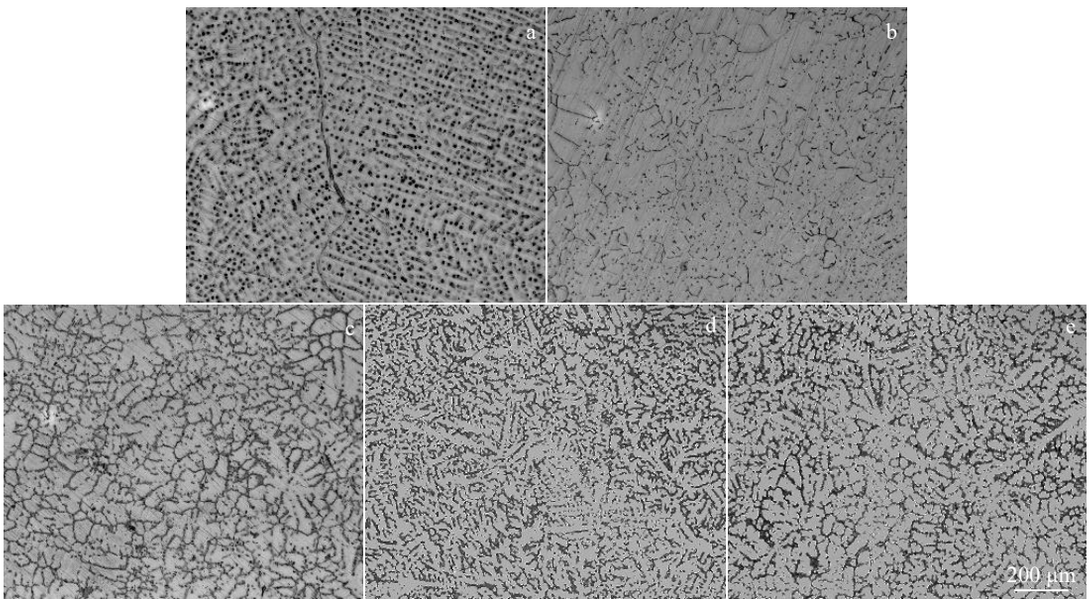

Fig.1 OM microstructures of as-cast Mg-2Zn-1Mn-*x*Y alloys: (a) *x*=0, (b) *x*=1, (c) *x*=3, (d) *x*=5, and (e) *x*=7

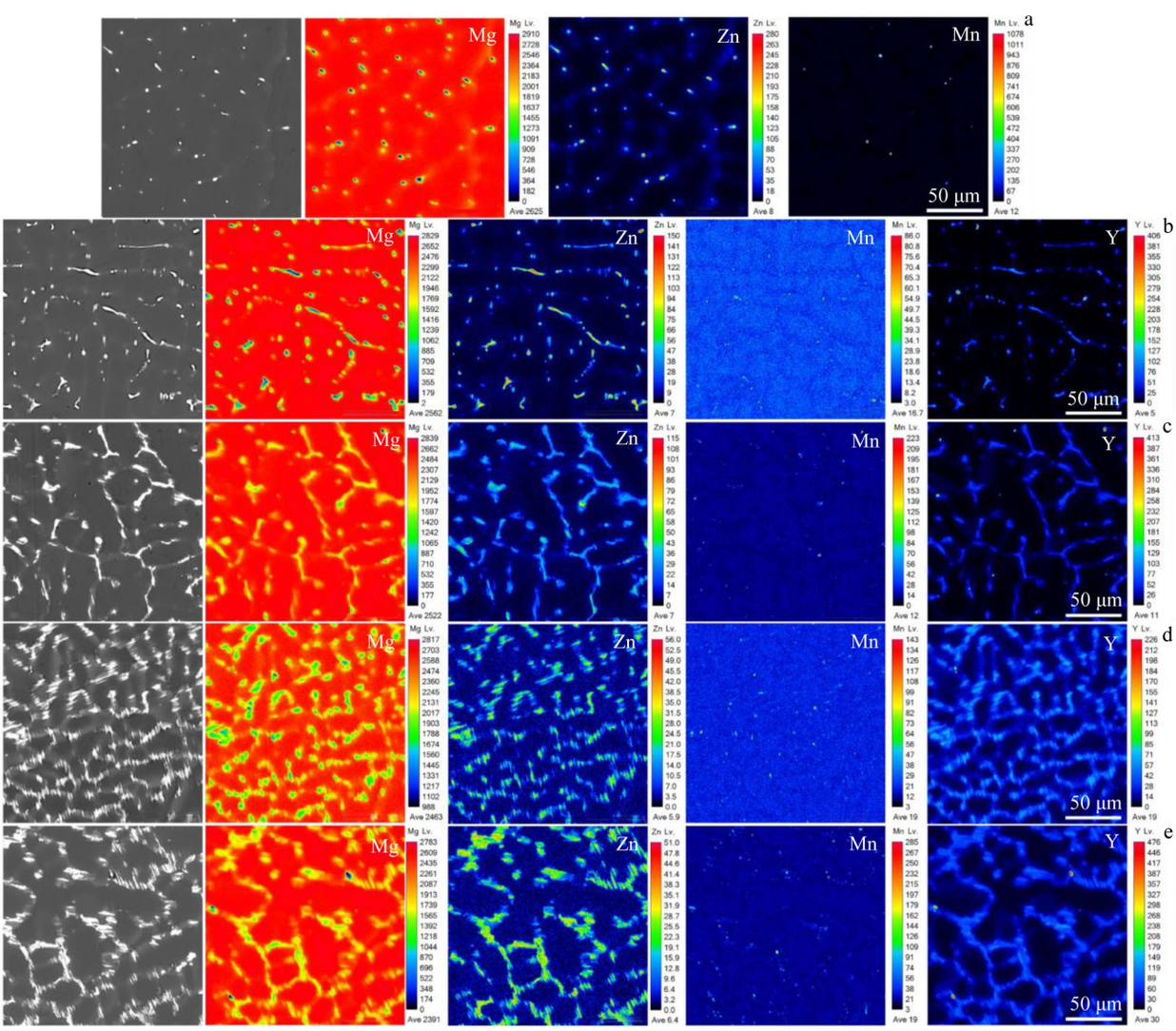

Fig.2 Bright phase particles morphologies and corresponding EPMA element mappings of as-cast Mg-2Zn-1Mn-*x*Y alloys: (a) *x*=0, (b) *x*=1, (c) *x*=3, (d) *x*=5, and (e) *x*=7

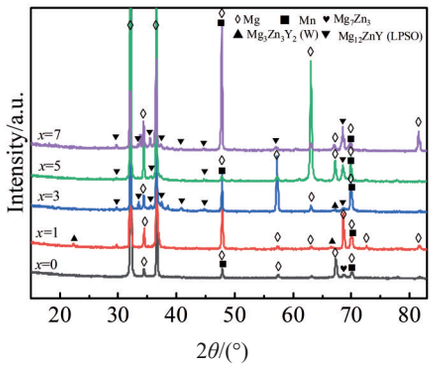

Fig.3 XRD patterns of different as-cast Mg-2Zn-1Mn-*x*Y alloys

extrusion and uniformly distributed along ED, as shown in Fig. 5b. The continuous lamellar LPSO-phase in as-cast microstructure was also crushed and elongated along ED. Moreover, with increasing the Y content, the spacing between LPSO-phase is dramatically decreased, and the volume fraction of coarse LPSO-phase is increased.

It is reported that the 18R structure is not thermodynamically stable at 500 ° C, and the 14H structure can gradually replace the 18R structure with prolonging the heat treatment duration at 500 ° C[24]. Therefore, to identify the structure of LPSO-phase, TEM observation was conducted, and the bright-field (BF) TEM images with corresponding selected area electron diffraction (SAED) patterns are shown

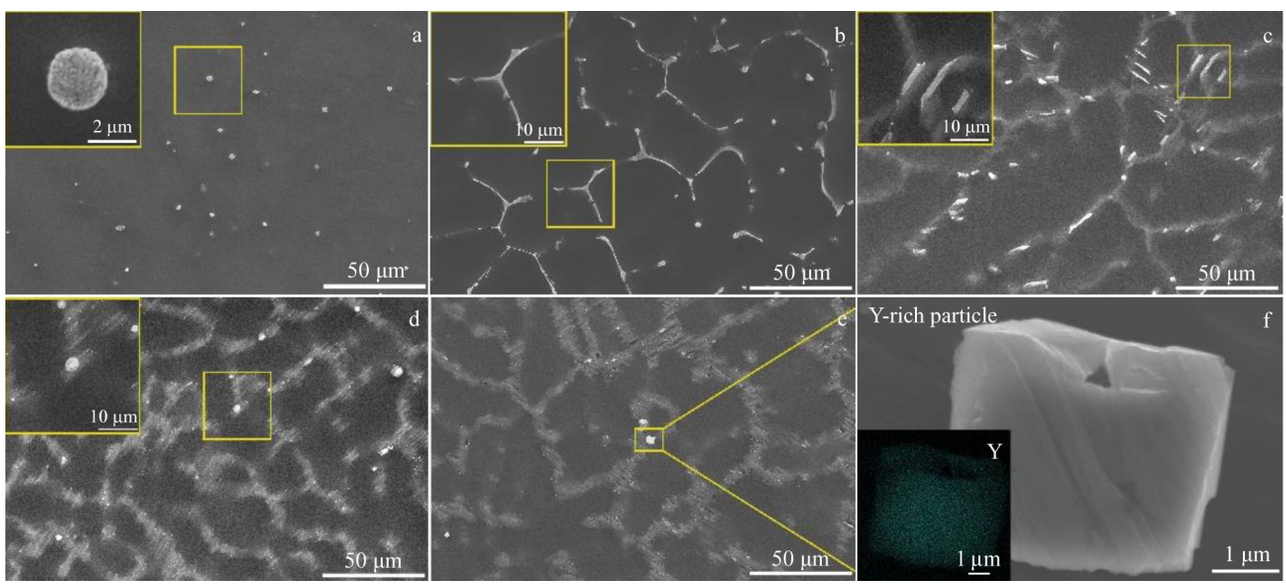

Fig.4 SEM microstructures of Mg-2Zn-1Mn-*x*Y alloys with *x*=0 (a), *x*=1 (b), *x*=3 (c), *x*=5 (d), and *x*=7 (e); magnified morphology of Y-rich particle in ZMW217 alloy and corresponding EDS mapping (f)

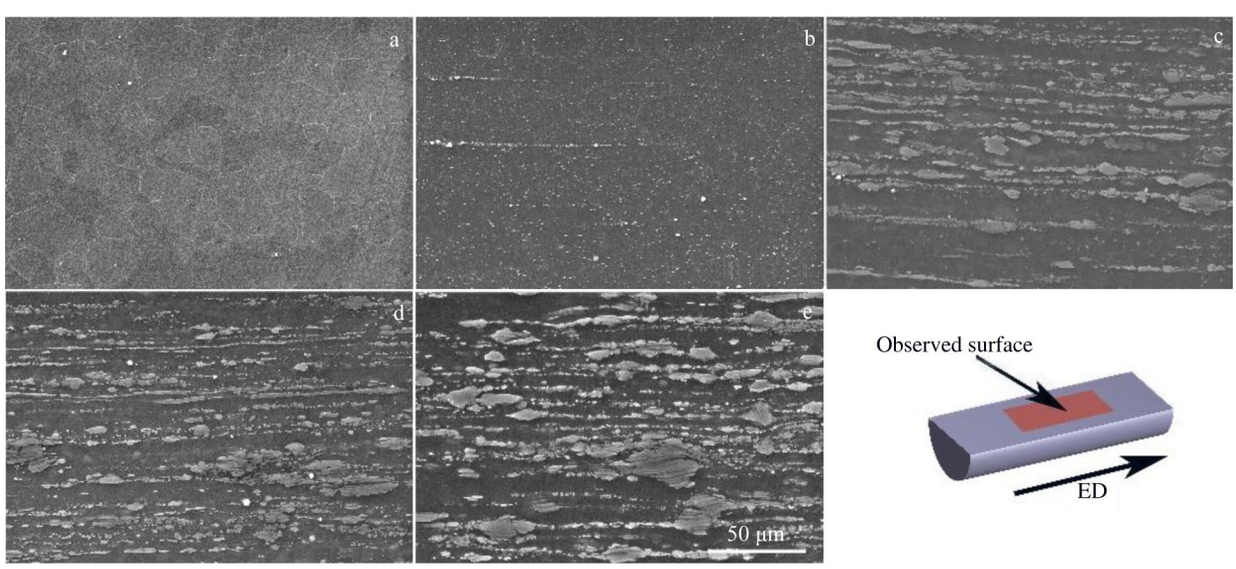

Fig.5 SEM microstructures of as-extruded Mg-2Zn-1Mn-*x*Y alloys: (a) *x*=0, (b) *x*=1, (c) *x*=3, (d) *x*=5, and (e) *x*=7

in Fig. 6. The LPSO-phase exhibits lamellar and bulk morphology, as shown in Fig. 6a. SAED patterns suggest that the block-shaped and lamellar LPSO-phases have 18R and 14H structures, respectively. In addition, the short lamellar structure can be observed between 14H-LPSO-phases, which can be identified as stacking faults (SFs) in α-Mg grains, as shown in Fig. 6d. In addition to the LPSO-phase, many granular secondary phases are distributed around the lamellar LPSO-phase. According to EDS element distributions of the region B in Fig. 6a, these granular secondary phases can be identified as the Mn particles.

Fig. 7 displays the evolution of inverse pole figures (IPFs) and pole figures (PFs) on the (0001) basal plane of as-extruded Mg-2Zn-1Mn-*x*Y alloys. The observed surface is parallel to ED, and different grain colors present different grain orientations in IPFs. After Y addition, the number of red and orange grains in IPFs reduces, indicating that the normal direction (ND) of most grains is far from <0001>. According to the (0001) PF, the basal pole of ZM21 alloy is distributed along the transverse direction (TD). With the Y addition, the polar axis of the {0001} PFs is inclined to ED. In addition, the orientations of most grains are $<01\bar{1}0>$//ED and $<\bar{1}2\bar{1}0>$//ED, and the texture intensity of Mg-2Zn-1Mn-*x*Y alloys reduces from 2.95 to 2.34, indicating that the basal texture weakens. The ZMW217 alloy exhibits the weakest basal texture, and texture intensity rapidly reduces to 2.34. It is reported that the orientations of dynamic recrystallized grains nucleated by PSN mechanism are more random than those of the parent grains, leading to easy activation of the $(0001)<11\bar{2}0>$ basal slip[25]. Therefore, the Y addition can effectively adjust the texture type of the magnesium alloys, which is beneficial to eliminate the adverse effect of basal texture.

In addition to the texture change of as-extruded alloys, the grain refinement can also be observed after the Y addition, as shown in Fig. 7. The average grain sizes of as-extruded Mg-2Zn-1Mn-*x*Y alloys with *x*=0, 1, 3, 5, and 7 are 9.5, 6.8, 3.6, 3.7, and 4.2 μm, respectively. This result indicates that the Y addition can significantly refine the grains with 1wt%−3wt% Y addition. The grain refinement is hindered with further increasing the Y content to 5wt% and 7wt%. The main reason for grain refinement is Y segregation and the secondary phase hinders the boundary migration of dynamic recrystallized grains. With increasing the Y addition, the volume fraction of the secondary phase is increased and the spacing between secondary phases is reduced, which decreases the hindrance effect of Y element on the growth of dynamic recrystallized grains, leading to the weakened grain refinement.

2.3 Mechanical properties of as-extruded Mg-2Zn-1Mn-*x*Y alloys

Fig. 8 shows the room temperature mechanical properties of Mg-2Zn-1Mn-*x*Y alloys. It is seen that the strength and EL exhibit different trends after Y addition. YS and UTS are increased with increasing Y content, and the maximum YS and UTS are achieved for the ZMW217 alloy, which is 262 and 357 MPa, respectively. However, EL is firstly increased and then reduced with increasing the Y content. When Y content increases to 3wt%, the maximum EL of 21% is obtained, which is 90% higher than that of ZM21 alloy. Then, the EL is gradually reduced to 14% with further increasing the Y addition to 7wt%. Therefore, it can be concluded that the ZMW217 alloy with YS of 262 MPa, UTS of 357 MPa, and EL of 14% has the optimal properties.

Grain refinement strengthening and secondary phase strengthening are common methods to strengthen the Mg and

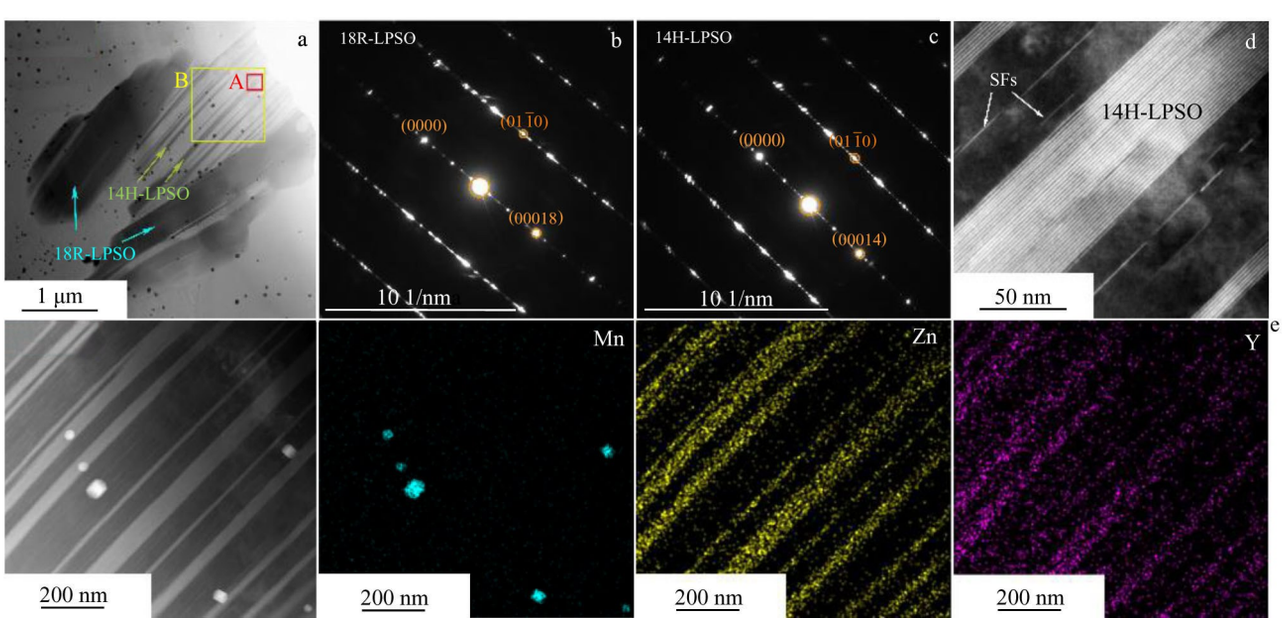

Fig.6 TEM BF images (a) and corresponding SAED patterns of 18R-LPSO-phase (b) and 14H-LPSO-phase (c) in as-extruded ZMW217 alloy; TEM HAADF image of region A in Fig. 6a (d); TEM image and EDS element distributions of region B in Fig. 6a (e) (electron beam is parallel to $[11\bar{2}0]_{Mg}$ in Fig.6b and 6c)

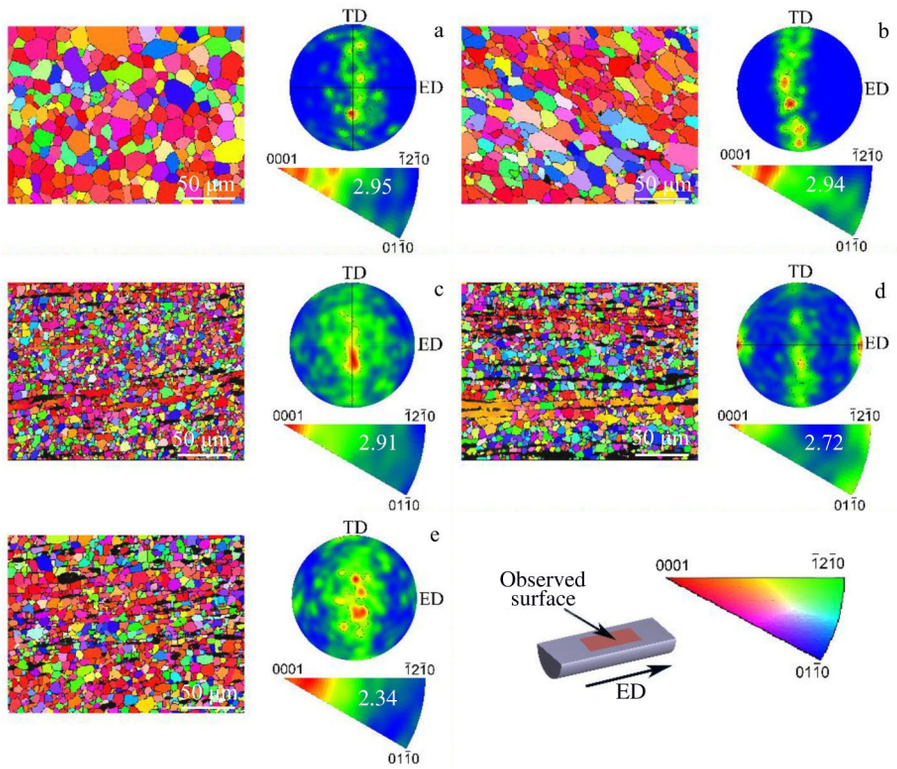

Fig.7 IPFs and PFs of (0001) basal plane of as-extruded Mg-2Zn-1Mn-*x*Y alloys: (a) *x*=0, (b) *x*=1, (c) *x*=3, (d) *x*=5, and (e) *x*=7

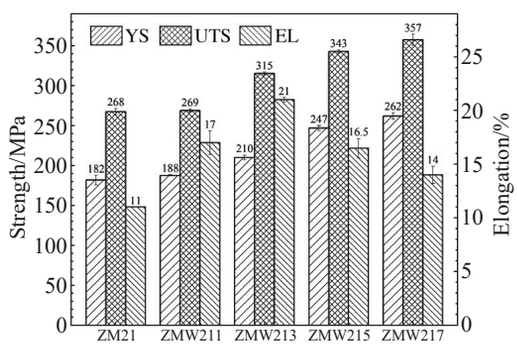

Fig.8 Mechanical properties of different as-extruded Mg-2Zn-1Mn-*x*Y alloys

its alloy. Based on Hall-Patch (HP) formula, $\sigma_s = \sigma_0 + k_y d^{-0.5}$ (d is the average grain diameter, σ_0 is the friction stress, σ_s is the stress, and k_y is the HP slope), YS is inversely proportional to the grain size, i.e., the finer the grains, the higher the YS[26]. According to the average grain size of Mg-2Zn-1Mn-*x*Y (*x*=0, 1, 3, 5, 7) alloys, it is inferred that the fine grain strengthening effect can be obtained by Y addition of 1wt%−3wt%, and it fails with further increasing the Y content. However, the strength of Mg-2Zn-1Mn-*x*Y alloys is continuously improved with Y addition, which can be attributed to the strengthening effect of secondary phase particles. The secondary phases in as-extruded alloys mainly contain W-phase and LPSO-phase. It is known that the particles of hard undeformed W-phase and LPSO-phase can pin the dislocation, resulting in the Orowan mechanism. Nevertheless, the strengthening caused by Orowan mechanism is largely related to the particle size, which can be significantly enhanced by reducing the particle size[27]. Tahreen et al[28] investigated the strengthening mechanism of I-phase, W-phase, and LPSO-phase. The contribution of W-phase induced by Orowan strengthening mechanism is stronger than that of LPSO-phase. Therefore, for the ZMW211 alloy, the strengthening effect of the secondary phase is mainly attributed to the fine dispersived W-phase. With increasing the Y content, the W-phase is replaced by LPSO-phase, and its contribution by Orowan strengthening mechanism is gradually reduced. However, the YS and UTS continuously increase. This result may be attributed to the unique strengthening effect of LPSO-phase. The hard brittle LPSO-phase has a coherent relationship with the α-Mg matrix, thereby improving the mechanical properties of alloys. However, different LPSO-phases have different strengthening effects. LPSO-phase can be categorized as 10R, 12H, 14H, and 18R structures[29–30]. Guo et al[31] investigated the influence of different LPSO-phases on the strengthening mechanism by the first-principle study, and reported that the 18R- and 14H-LPSO-phases are the main strengthening phases. Therefore, the LPSO-phase mainly consists of the 14H- and 18R-LPSO-phases. Particularly, the blocky 18R-LPSO-phase distributed at the grain boundaries can prevent the dislocation slip and cause the dislocation pile-up, thereby enhancing the alloy properties[32]. Meanwhile, the strengthening effect is enhanced with increasing the volume fraction of LPSO-phase[33]. According to Fig. 8, the strength of alloy with W-phase is worse than that of alloy with LPSO-phase, which indicates

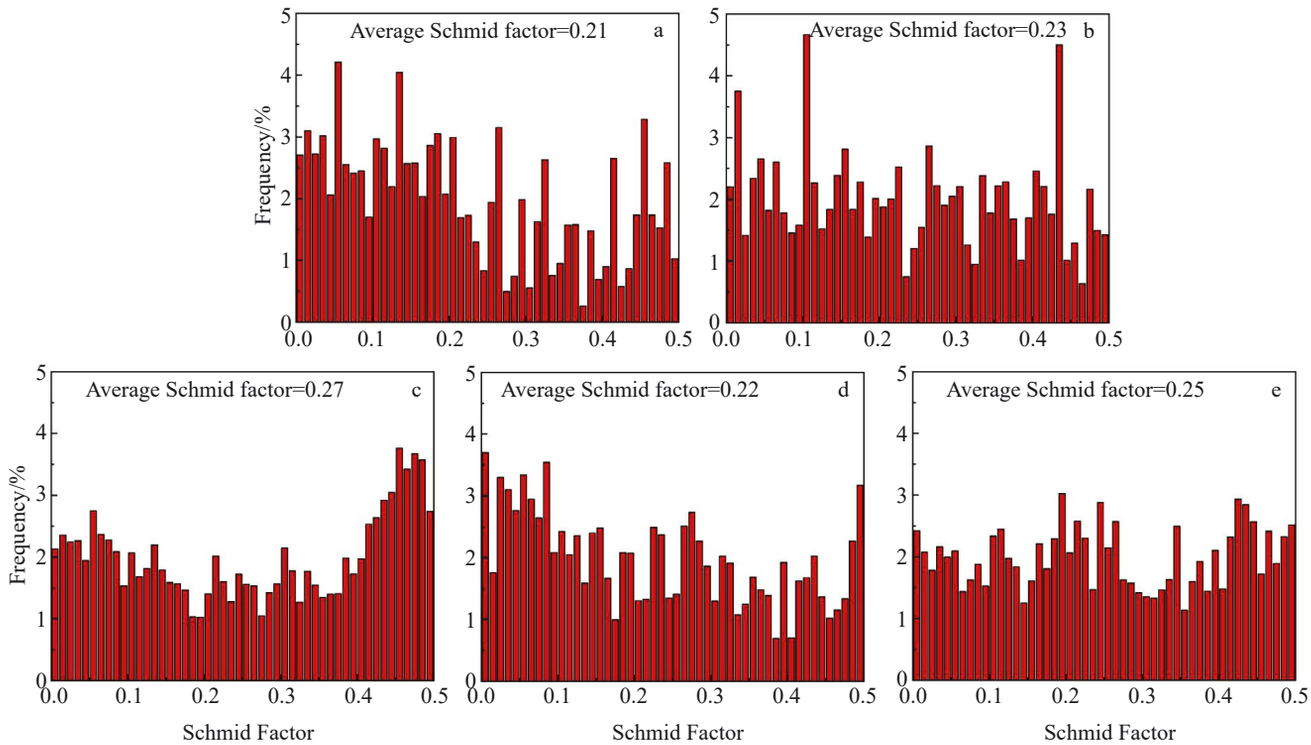

Fig.9 Schmid factor distributions of (0001)<11$\bar{2}$0> basal slip in as-extruded Mg-2Zn-1Mn-*x*Y alloys: (a) *x*=0, (b) *x*=1, (c) *x*=3, (d) *x*=5, and (e) *x*=7

that the strengthening effect contributed by LPSO-phase is greater than that by W-phase. This result is consistent with the results in Ref. [34]. The ZMW217 alloy possesses the relatively refined grains and the maximum amount of LPSO-phase, thus exhibiting the optimal strength.

The ductility is mainly influenced by the grain size, texture components, slip modes, and secondary phase. For the fine grains, the strain difference between the internal grain and the grain near the grain boundary is slight, and the deformation is more uniform under the same loading. Therefore, the chance of cracking caused by stress concentration decreases, leading to a higher ductility[3]. The secondary phase particles also play an important role to affect the ductility of Mg alloys. For the as-extruded ZMW211 alloy, the broken fine W-phase particles distributed along ED during hot extrusion can improve the mechanical properties through the grain refinement and weakening of basal texture[20]. In addition, the highly-coherent interface between the magnesium matrix and LPSO-phase and the inhibition effect of kink structure of LPSO-phase on debonding or micro-cracking propagation are both beneficial to the enhancement of ductility and strength[15,35]. Hence, ZMW213 alloy has the optimal EL of about 21% due to the presence of LPSO-phase. It is worth noting that once the Y content is more than 3wt%, EL begins to decrease. When the Y addition exceeds 3wt%, the grain size increases slightly, resulting in the weakened improvement effect of grain refinement on ducitility.

The wrought Mg alloys have obvious anisotropy and poor formability at room temperature due to the strong basal texture formed during extrusion[3]. According to the abovementioned results, more random crystallization orientations of grains are obtained after the Y addition, and thus the high ductility of alloys is obtained. The basal slip is the dominant deformation mode in Mg alloys. It is reported that the difficulty degree of activation of basal slip can be evaluated by the Schmid factor[36]. Long et al[37] reported that the basal <a> slip is promoted after the Y addition, while the Y addition has a little effect on pyramidal slip system. Fig. 9 presents the Schmid factor distribution of (0001)<11$\bar{2}$0> basal slip in as-extruded Mg-2Zn-1Mn-*x*Y alloys under the uniaxial deformation along ED. Obviously, the average Schmid factor of the ZMW213 alloy is the maximum, suggesting that basal slip is easier to activate under the applied stress, leading to the high ductility but low strength of ZMW213 alloy. The average Schmid factor is reduced with further increasing the Y addition. The grains with Schmid factor of less than 0.2 account for 38% and 40% in ZMW213 and ZMW217 alloys, respectively; the grains with Schmid factor of greater than 0.4 account for 30% and 23% in ZMW213 and ZMW217 alloys, respectively. This result indicates that the number of grains with soft orientation in ZMW213 alloy is more than that in ZMW217 alloy, which leads to better ductility of ZMW213 alloy. In conclusion, although the Y addition can effectively improve the strength and ductility of ZM21 alloy, when the addition amount is more than 3wt%, the positive effect of Y addition on grain refinement and ductility is reduced. Meanwhile, the ZMW217 alloy has the optimal properties of strength and ductility: YS, UTS, and EL are 262 MPa, 357

MPa, and 14%, respectively.

3 Conclusions

1) The as-cast Mg-2Zn-1Mn (ZM21) alloy consists of α-Mg, Mn, and Mg_7Zn_3 phases. With increasing the Y content, the $Mg_3Zn_3Y_2$ (W-phase) and $Mg_{12}ZnY$ (LPSO-phase) can be detected. The Y addition can refine the grains, but the refinement degree is inferior with excess addition of Y element.

2) The Y addition results in more refined grains, which hinders the dynamic crystallization process. All as-extruded Mg-2Zn-1Mn-*x*Y alloys exhibit the typical basal texture, and the Y addition decreases the texture intensity.

3) The Y addition improves the mechanical properties at room temperature of as-extruded ZM21 alloy. The strength is continuously increased with increasing the Y content due to the grain refinement strengthening and the secondary phase strengthening.

4) The ductility of Mg-2Zn-1Mn-*x*Y alloys is firstly increased and then decreased with increasing the Y content due to the variation in grain size and texture orientation. As a result, the Mg-2Zn-1Mn-7Y alloy exhibits the optimal properties of strength and ductility: yield strength, ultimate tensile strength, and elongation are 262 MPa, 357 MPa, and 14%, respectively.

References

1 Pan H C, Ren Y P, Fu H *et al*. *Journal of Alloys and Compounds* [J], 2016, 663: 321

2 Song J F, She J, Chen D L *et al*. *Journal of Magnesium and Alloys*[J], 2020, 8(1): 1

3 Zhao Y, Zhang D F, Xu J Y *et al*. *Intermetallics*[J], 2021, 132: 107 163

4 Zhang D F, Shi G L, Zhao X B *et al*. *Transactions of Nonferrous Metals Society of China*[J], 2011, 21(1): 15

5 Bazhenov V E, Li A V, Komissarov A A *et al*. *Journal of Magnesium and Alloys*[J], 2021, 9(4): 1428

6 Liang M J, Chen Z, Zhang J X *et al*. *Transactions of Nonferrous Metals Society of China*[J], 2008, 18(1): 59

7 Yin D S, Zhang E L, Zeng S Y. *Transactions of Nonferrous Metals Society of China*[J], 2008, 18(4): 763

8 Pan F S, Mao J J, Zhang G *et al*. *Progress in Natural Science: Materials International*[J], 2016, 26(6): 630

9 She J, Peng P, Xiao L *et al*. *Materials Science and Engineering A*[J], 2019, 765: 138 203

10 Hu G S, Xing B, Huang F L *et al*. *Journal of Alloys and Compounds*[J], 2016, 689: 326

11 Hu G S, Zhang D F, Tang T *et al*. *Materials Science and Engineering A*[J], 2015, 634: 5

12 Ye Z J, Teng X Y, Luo G *et al*. *Materials Research Express*[J], 2017, 4(8): 86 502

13 Wu X F, Xu C H, Zhang Z W *et al*. *Advanced Engineering Materials*[J], 2020, 22(3): 1 900 964

14 Li C Q, Xu D K, Zeng Z R *et al*. *Materials and Design*[J], 2017, 121: 430

15 Shao X H, Yang Z Q, Ma X L. *Acta Materialia*[J], 2010, 58(14): 4760

16 You S H, Huang Y D, Kainer K U *et al*. *Journal of Magnesium and Alloys*[J], 2017, 5(3): 239

17 Yoshimoto S, Yamasak M, Kawamura Y. *Materials Transactions* [J], 2006, 47(4): 959

18 Hao J Q, Zhang J S, Li B Q *et al*. *Materials Science and Engineering A*[J], 2021, 804: 140 727

19 Xu D K, Tang W N, Liu L *et al*. *Journal of Alloys and Compounds*[J], 2008, 461(1–2): 248

20 Wang Q F, Liu K, Wang Z H *et al*. *Journal of Alloys and Compounds*[J], 2014, 602: 32

21 Chen R, Xu J Y, Zhang D F *et al*. *Rare Metal Materials and Engineering*[J], 2019, 48(7): 2084

22 Nodooshan H R J, Liu W C, Wu G H *et al*. *Materials Science and Engineering A*[J], 2014, 615: 79

23 Honma T, Ohkubo T, Hono K *et al*. *Materials Science and Engineering A*[J], 2005, 395(1–2): 301

24 Zhu Y M, Morton A J, Nie J F. *Acta Materialia*[J], 2010, 58(8): 2936

25 Zhao T S, Hu Y B, He B *et al*. *Materials Science and Engineering A*[J], 2019, 765: 138 292

26 Pan H C, Qin G W, Huang Y M *et al*. *Acta Materialia*[J], 2018, 149: 350

27 Zhang Z, Chen D L. *Materials Science and Engineering A*[J], 2008, 483–484: 148

28 Tahreen N, Zhang D F, Pan F S *et al*. *Journal of Materials Science and Technology*[J], 2018, 34(7): 1110

29 Liu C, Zhu Y M, Luo Q *et al*. *Journal of Materials Science and Technology*[J], 2018, 34(12): 2235

30 Guo Y L, Li Y, Liu B *et al*. *Journal of Alloys and Compounds*[J], 2018, 750: 117

31 Guo Y L, Luo Q, Liu B *et al*. *Scripta Materialia*[J], 2020, 178: 422

32 Wang D, Wu H J, Wu R Z *et al*. *Journal of Magnesium and Alloys*[J], 2020, 8(3): 793

33 Tong L B, Li X H, Zhang H J. *Materials Science and Engineering A*[J], 2013, 563: 177

34 Zhu J, Chen X H, Wang L *et al*. *Journal of Alloys and Compounds*[J], 2017, 703: 508

35 Tahreen N, Zhang D F, Pan F S *et al*. *Journal of Alloys and Compounds*[J], 2015, 644: 814

36 Xia D B, Chen X, Huang G D *et al*. *Scripta Mater*[J], 2019, 171: 31

37 Long L J, Huang G H, Yin D D *et al*. *Metallurgical and Materials Transactions A*[J], 2020, 51(6): 2738

高Y添加量对Mg-2Zn-1Mn合金组织和力学性能的影响

罗宇伦[1,2]，张丁非[1,2]，华建荣[1,2]，代啟敏[1,2]，钟诗宇[1,2]，胥钧耀[1,2]，胡光山[3]，蒋　斌[1,2]，潘复生[1,2]

(1. 重庆大学 材料科学与工程学院，重庆 400045)

(2. 重庆大学 国家镁合金材料工程技术研究中心，重庆 400044)

(3. 嘉兴学院 信息科学与工程学院，浙江 嘉兴 314001)

摘　要：采用光学显微镜、X射线衍射仪、X射线荧光法、电子探针显微分析仪、扫描电子显微镜、电子背散射衍射、透射电子显微镜和单轴拉伸测试等对Mg-2Zn-1Mn-*x*Y (*x*=0，1，3，5，7，质量分数，%)合金的显微组织和力学性能进行研究。结果表明：随着Y元素的加入，铸态合金的第二相由Mg_7Zn_3转变为$Mg_3Zn_3Y_2$，最终转变为$Mg_{12}ZnY$。Y元素的加入阻碍了动态再结晶的生长过程，使晶粒得到细化，但是进一步增加Y含量不会继续增强晶粒细化程度。挤压态Mg-2Zn-1Mn合金加入Y元素后，塑性呈现出先升高后下降的趋势，这可能是受到了织构取向变化和晶粒粗化的共同影响。此外，合金强度提高主要是由于细晶强化和第二相强化作用。Mg-2Zn-1Mn-7Y合金具有最佳的力学性能，其抗拉伸强度为357 MPa，屈服强度为262 MPa，延伸率为14%。

关键词：Mg-Zn-Mn-Y；组织；性能；织构

作者简介：罗宇伦，男，1995年生，硕士，重庆大学材料科学与工程学院，重庆 400044，E-mail：luoyulun@cqu.edu.cn